This is the peer reviewed version of the following article: Ballo, F., Frizzi, R., Mastinu, G., Mastroberti, D. et al., "Lightweight Design and Construction of Aluminum Wheels," SAE Technical Paper 2016-01-1575, which has been published in final form at http://dx.doi.org/10.4271/2016-01-1575

Lightweight Design and Construction of Aluminum Wheels

Federico Ballo [1], Roberto Frizzi [2], Gianpiero Mastinu [1], Donato Mastroberti [2], Giorgio Previati [1], Claudio Sorlini [2]

[1]Politecnico di Milano, [2]Cromodora Wheels

Abstract

In this paper the lightweight design and construction of road vehicle aluminum wheels is dealt with, referring particularly to safety. Dedicated experimental tests aimed at assessing the fatigue life behavior of aluminum alloy A356 - T6 have been performed. Cylindrical specimens have been extracted from three different locations in the wheel. Fully reversed strain-controlled and load-controlled fatigue tests have been performed and the stress/strain-life curves on the three areas of the wheel have been computed and compared. The constant amplitude rotary bending fatigue test of the wheel has been simulated by means of Finite Element method. The FE model has been validated by measuring the strain at several points of the wheel during the actual test. From the FE model, the stress tensor time history on the whole wheel over a loading cycle has been extracted. The Sines fatigue criterion and the critical plane approach have been adopted for computing the fatigue life of the wheel and results have been compared with the fatigue tests on the actual component. Both of the two criteria underestimate the life of the component. A proper criterion to assess such a discrepancy is proposed. The process of wheel construction which guarantees the repeatability of experimental tests is highlighted.

Introduction

The present project comes from the collaboration between Politecnico di Milano (Technical University of Milan, Italy) and Cromodora Wheels [38].

Weight reduction is a central task in vehicles design and nowadays is taking on an even greater importance in road vehicles development. Automotive OEM's and components manufacturers are performing several research activities to reduce the mass of the vehicles. Mass reduction is a central issue in the design of new road vehicles, not only for improving vehicle performances, but also for the reduction of fuel consumption and emissions, to cope with the more recent and demanding international regulations. Minimizing the overall mass of a vehicle means minimizing the mass of each single component.

Besides mass minimization, acceptable structural performances and safety requirements have to be guaranteed [31, 32].

In automotive engineering, wheels are critical components and are of primary importance for safety. Significant efforts have been devoted by Wallace et al. for obtaining standard test methods that guarantee safety requirements of vehicles wheels in [33, 34]. Lightweight design assumes an even greater importance if applied to vehicle wheels, in fact reducing the unsprung mass provides important advantages in terms of ride comfort and handling [1, 2, 30].

Aluminum wheels are nowadays mounted on the large majority of medium and premium class vehicles. The cyclic nature of in-service loading makes fatigue performances one of the most critical aspect related to safety of such a component. The knowledge of in-service loading spectra is also a key factor for the design of vehicles wheels [1, 24]. The capability of measuring forces acting on the wheel during real working conditions is therefore a valuable tool for the design of such a component. In this framework, many examples of three-components [25] and six-components [16, 26,27,28,29] wheel force sensors can be found in the literature. In this paper fatigue life prediction of A356 cast-aluminum wheels is discussed. Fatigue performances of aluminum wheels depend on many factors like the surface finishing, manufacturing process, heat treatment, defects and microstructure, loading condition etc. [3, 4]. Moreover, for castaluminum wheels, fatigue properties may be different in the various areas of the wheel, because of the different solidification processes and defects concentration [35,36,37]. In order to account of these effects, fatigue properties of the material have been evaluated on specimens machined out from different zones of an actual wheel [5].

Due to the complexity of the geometry of a cast-aluminum wheel, finite element-based methods are generally employed for predicting fatigue life [5,6,7,8,9, 21,22,23]. The complex stress field in the wheel requires the application of multiaxial fatigue criteria for durability assessment. Roughly speaking two main different approaches can be identified for estimating fatigue performances of wheels, namely stress-based and strain-based approaches. Stress-based methods start from the computation of the stress field on the component, an equivalent stress is computed from the local stress-tensor and compared with the S-N curve of the material. The total fatigue life of the wheel is obtained by applying the Palmgrem-Miner rule [5, 6, 13]. Strain-based methods on the other hand are mostly concerned with the local strain field in the component. These approaches are based on the assumption that the period to crack initiation is governed by the strain field at the notch [7,8,9]. The cyclic behavior of the material is considered.

In this work the rotary cornering fatigue test has been simulated by means of finite element method in order to predict the fatigue life of the wheel. The test procedure is outlined in the SAE J328 standard wheel test [12] - the wheel is fixed at the inner side of the rim and a constant rotating bending moment is applied at the central hub. Dealing with a complex stress state, multiaxial fatigue criteria have been employed for computing the fatigue life of the wheel. Since the stress levels in the wheel are within the elastic region of the material for the considered loading condition, a stress-based approach has been followed.

The paper is structured as follows. The fatigue tests aimed at assessing the fatigue properties of the material are described in the first section. The subsequent section is dedicated to the numerical model developed for simulating the bending fatigue test together with the experimental validation. Then multiaxial fatigue criteria have been employed for estimating the fatigue life of the wheel. A correction of the limit stress of the material according to the stress gradient at the notches is proposed.

Material Fatigue Properties

Experimental tests aimed at evaluating the fatigue properties of the material have been performed. The specimens have been extracted from a set of wheels subjected to the same manufacturing process. Three different zones on the wheel have been selected for extracting the specimens as shown in Figure 1.

Fully reversed strain-controlled and load-controlled axial fatigue tests have been performed on cylindrical specimens with diameter of 6 mm. The specimens have been prepared according to the guidelines of the ASTM and ISO standards for strain-controlled fatigue tests [10, 11]. Specimens have been obtained by cylindrical grinding followed by a final polishing for obtaining a surface roughness of 0.3 μm.

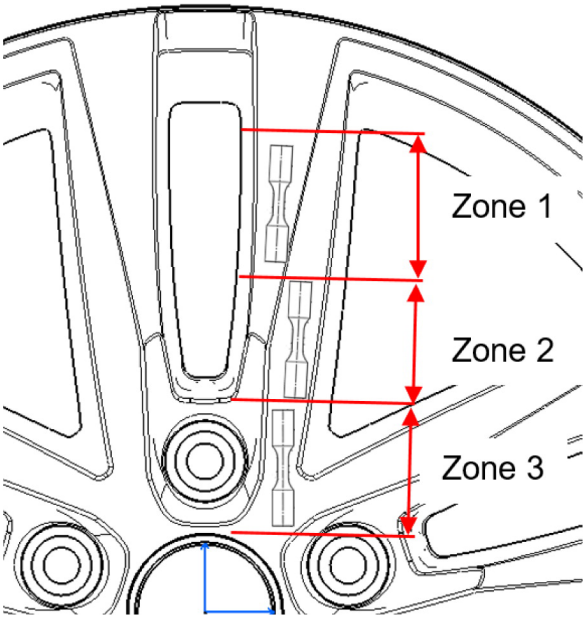

Figure 1. Different locations of extraction of the specimens.

For each of the three zones, 5 different strain amplitudes have been tested, namely 0.1%, 0.2%, 0.3%, 0.4% and 0.5%. A total of 45 specimens (15 per zone) have been tested. The strain levels below 0.2% have been obtained by controlling the axial load at a frequency of 30 Hz. For the remaining strain amplitudes the tests were conducted by controlling the axial strain at a rate of 0.5 Hz. The tests have been performed on a MTS Landmark hydraulic axial testing machine at the Politecnico di Milano (Technical University of Milan), Italy.

The stress and strain-life curves have been obtained for each of the analyzed zones. Figure 2 shows the strain-life curve obtained from specimens extracted from zone 2 of the wheel.

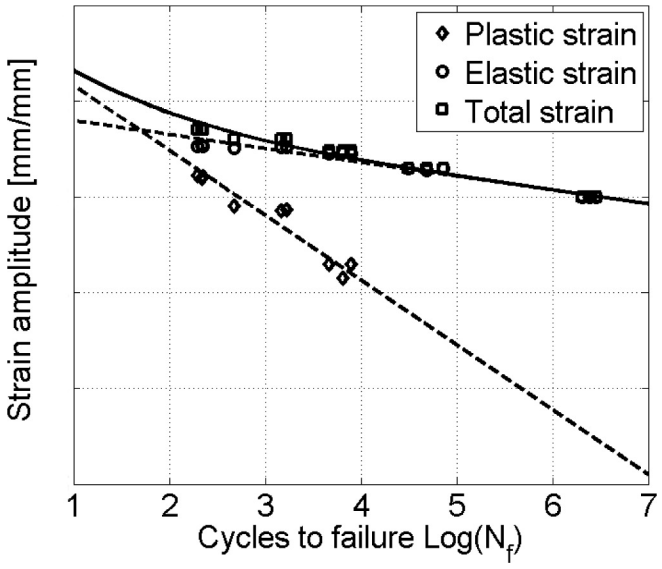

Figure 2. Strain-life curve obtained from specimens extracted from zone 2.

The comparison between the obtained curves is shown in Figure 3, where it emerges that there are no significant differences for medium/ high number of cycles, while the curve of zone 3 tend to differ in the low cycle region.

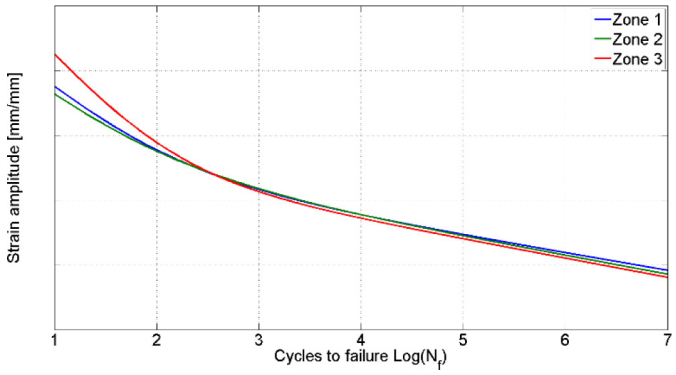

Figure 3. Comparison of the strain-life curves for the three specimens extracted from the three different zones of the wheel shown in Fig.1.

The stress-life curve does not exhibit significant differences among the three zones of the wheel (Figure 4). The stress-life curve was obtained from the Basquin's equation [15]:

$$\sigma_a = \sigma_f^{'}\left(2N_f\right)^b \qquad (1)$$

where σ_a is the amplitude of the alternate stress, σ'_f and b are the fatigue strength coefficient and the fatigue strength exponent respectively.

The stress-life curve is valid only in case the stresses on the wheel are within the elastic region, i.e. in the high cycle fatigue region.

By inspecting the fracture surfaces, it was found that the fatigue damage was mainly due to the presence of porosities.

The small variability of material fatigue properties in the wheel confirm the effectiveness of the whole die-casting process.

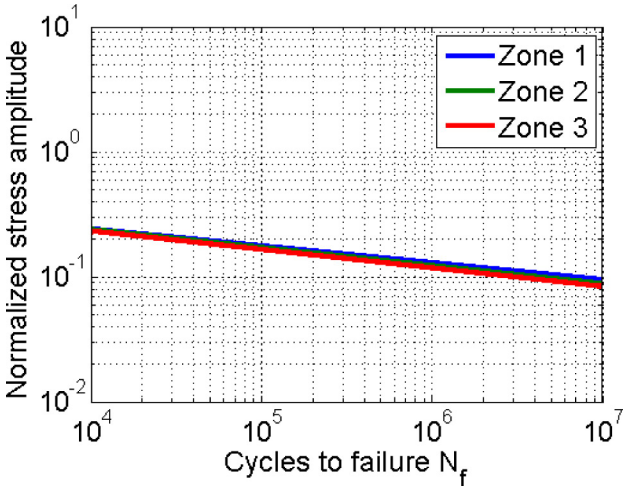

Figure 4. Comparison of the stress-life curves for the three specimens extracted from the three zones of the wheel shown in Fig.1 - stress amplitudes are normalized by the maximum stress.

Numerical Model and Experimental Validation

The constant amplitude rotary cornering fatigue test [12] of the wheel has been simulated by means of Finite Element method. In the fatigue test the wheel is fixed on one side of the rim and a rotating bending moment is applied at the central hub via a rotating eccentric mass (Figure 5).

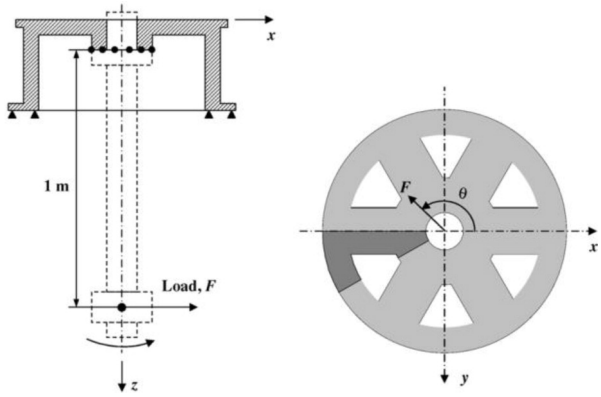

(a). (b).

Figure 5. Scheme of the rotating bending fatigue test, adapted from [3].

FE Model of the Wheel

The solid model of the wheel has been discretized with a finite element mesh, 10 node tetrahedral elements have been employed. The global size of the element was 6 mm, with a progressive refinement down to 1 mm at fillets between the spokes and the central hub as shown in Figure 6.

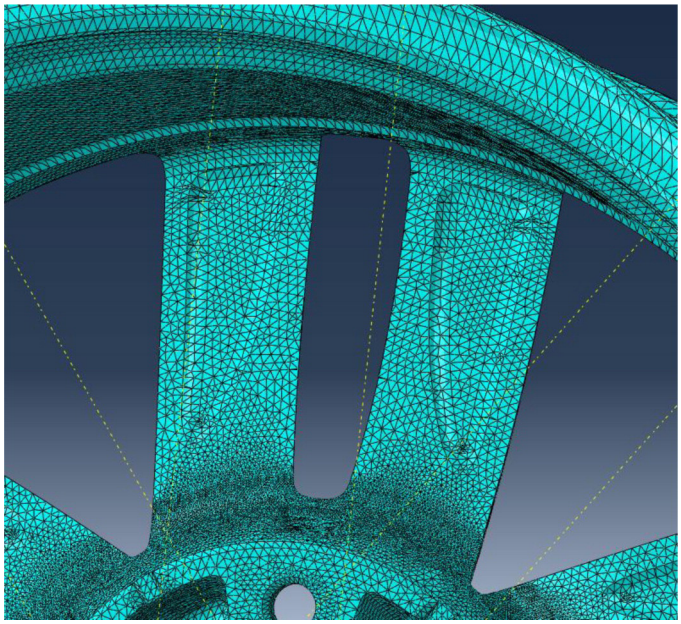

Figure 6. Finite element mesh, global size 6mm with a progressive refinement at the central hub.

The wheel is constrained at one side of the external rim as depicted in Figure 7.

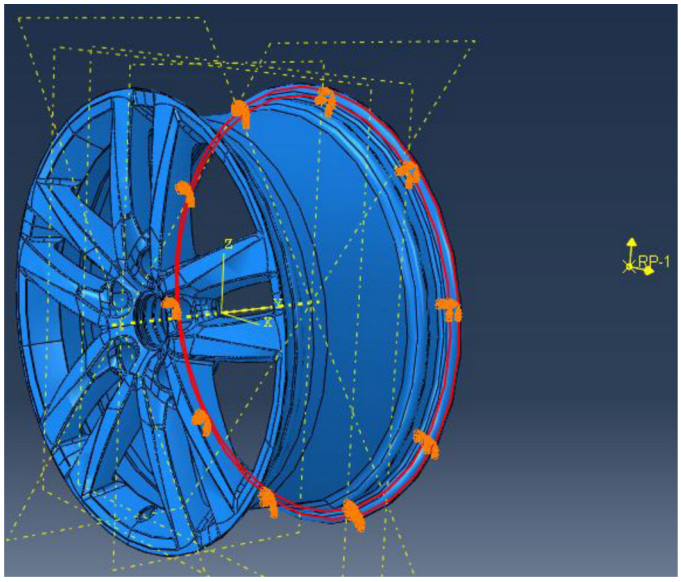

Figure 7. Constraint scheme and loads applied to the wheel.

The bending load has been applied at a point rigidly connected with the coupling flange of the wheel (Figure 7). A complete revolution of the bending moment has been simulated and the strain and stress tensors histories on the entire wheel over a loading cycle have been extracted. Figure 8 shows an example of the evolution of the six components of the stress tensor in a point of the wheel over a complete revolution of bending moment.

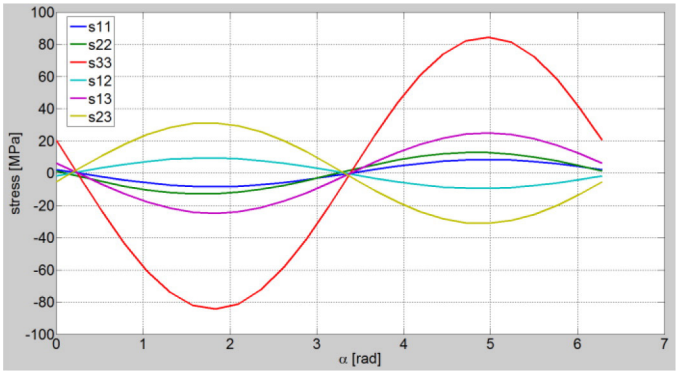

Figure 8. Time history of stress components at a point of the wheel over a loading cycle.

Experimental Validation

The implemented FE model has been experimentally validated. An actual wheel has been instrumented with 8 strain gauges located at the most stressed areas. Strain gauges have been applied on front and rear surface of the wheel as shown in Figure 9-10. Uniaxial resistive strain gauges have been mounted on the spokes, where stresses in transversal direction are low. A strain rosette was employed in the zone near the fillet between the spoke and the hub where a multiaxial stress state is present.

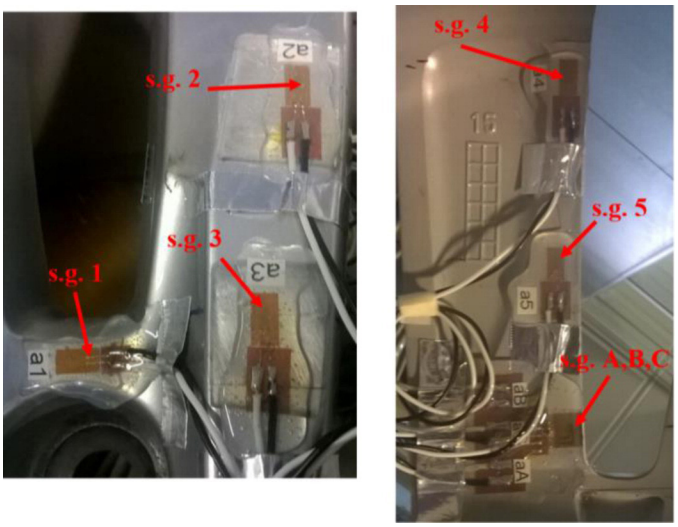

Figure 9. Strain gauges located at the most stressed areas of the wheel.

The wheel has been mounted on the rotary fatigue test bench (Figure 10) and the eight signals have been acquired at a sampling frequency of 400 Hz.

The acquired signals have been compared with the numerical simulations. Different loading levels have been explored, namely 4000, 6000 and 8000 Nm, a good agreement has been obtained with a maximum difference below 10% of the maximum measured strain as reported in Table 1.

Figure 10. Instrumented wheel mounted on the rotary fatigue test bench.

Table 1. Percentage errors between numerical simulations and experimental data.

Strain gauge	4000 Nm	6000 Nm	8000 Nm
1	5.5%	7.4%	9.2%
2	1.4%	1.1%	1.7%
3	1.6%	1.4%	0.9%
4	5.5%	6.6%	7.6%
5	0.8%	0.3%	1.2%
A	5.5%	2.7%	4.9%
B	8.6%	5.9%	8%
C	6.5%	7.3%	7.3%

Fatigue Life Prediction

The validated FE model has been used for the computation of the fatigue life of the wheel subjected to the rotary bending fatigue test. The fatigue test has been simulated and the stress tensor history over a loading cycle has been extracted at each integration point. Two different fatigue criteria have been implemented and compared, namely the Sines and critical plane (Matake) criterion.

The Sines criterion is based on a stress invariant approach [14]. The criterion is valid for in-phase loading, i.e. principal directions do not change during the loading cycle. An equivalent stress is obtained as

$$\sigma_S = \frac{1}{b_2}\frac{\sqrt{\sigma_{Ia}{}^2+\sigma_{IIa}{}^2+\sigma_{IIIa}{}^2-(\sigma_{Ia}\sigma_{IIa}+\sigma_{IIa}\sigma_{IIIa}+\sigma_{Ia}\sigma_{IIIa})}}{1-\frac{I_{1m}}{\sigma_u}} \quad (2)$$

Where at the numerator we have the amplitudes of the principal stresses, while the denominator accounts for the effect of mean stress (I_{1m} is the mean value of the first invariant of the stress tensor while σ_u is the ultimate stress). The b_2 coefficient (< 1) expresses the effect of the surface finishing. For this application a value of 0.9, taken from the literature [6], has been considered. From the calculated equivalent stress the limit number of cycles can be obtained from the experimental Wöhler's curve of the material [15, 16].

The critical plane approach on the other hand, looks for the most critical direction in the material, i.e. the plane on which the damage nucleates. Several criteria based on the critical plane approach have been proposed [14, 17], in this work the Matake criterion has been adopted. The critical plane is defined by the plane where the maximum shear stress amplitude is exerted. The Matake equivalent stress reads

$$\sigma_{Matake} = \frac{1}{b_2}\left(\tau_{c,a}+\left(2\frac{\tau_{af}}{\sigma_{af}}-1\right)\sigma_{c,a}\right) \quad (3)$$

being $\tau_{c,a}$ the shear stress amplitude acting on the critical plane, τ_{af} and σ_{af} the torsional and axial fatigue limits respectively and $\sigma_{c,a}$ the amplitude of the normal stress on the critical plane.

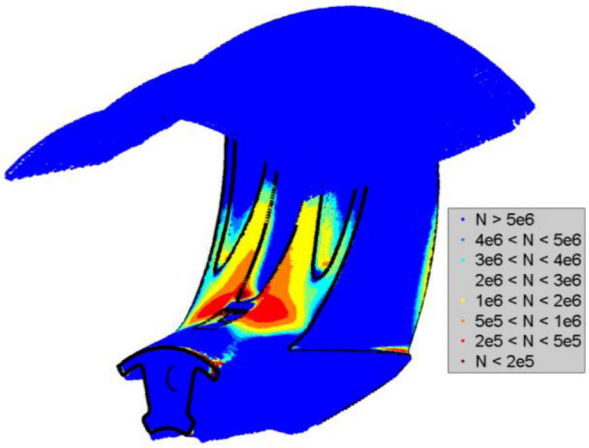

Figure 11. Contour plot of the fatigue life of the wheel computed with the Sines criterion.

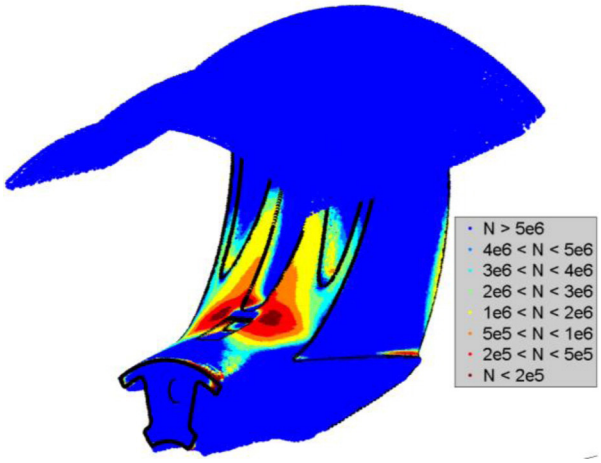

Figure 12. Contour plot of the fatigue life of the wheel computed with the Matake criterion.

Once the equivalent stresses are computed the fatigue life of the wheel can be calculated. Figure 11 and Figure 12 show the fatigue life of the wheel computed with the two methods.

Both of the methods converge on the location of the damage and on the number of cycles. The critical plane approach predicts a slightly lower fatigue life than the Sines criterion. The estimated fatigue life around the critical area is about $3 \cdot 10^5$ and $4.5 \cdot 10^5$ cycles respectively. This difference can be explained by the fact that the stress components in the wheel do not vary in a purely proportional way, but there is a limited phase shift in some areas.

Results from experimental tests show that the location of the damage is well captured by the numerical methods as shown in Figure 13. Both the two methods seem to underestimate the fatigue life of the wheel.

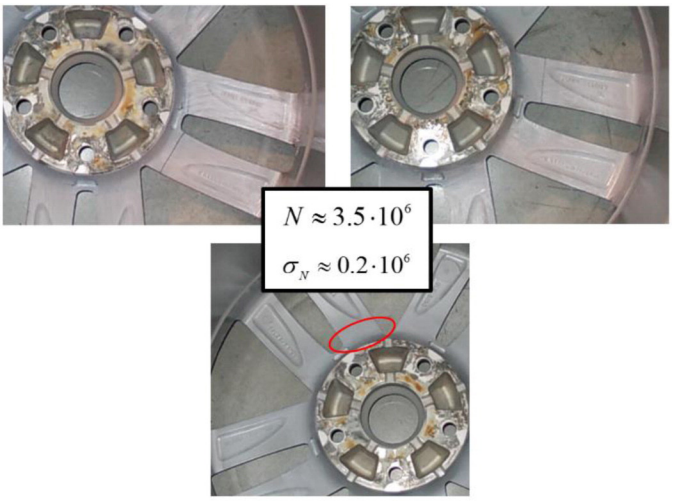

Figure 13. Cracks after a rotary bending fatigue test on three different wheels.

The Effect of Local Stress Gradient

In general the stress-life curves of materials are derived from tension-compression loading of unnotched specimens. However actual components are characterized by a massive presence of notches. Notches are characterized by an increase in the stress and stress gradient within the component. In presence of notches material exhibits higher fatigue stress limits than in the case of pure tensile loading on unnotched specimens [18]. This effect is expressed by the so-called *notch support factor*. The notch support factor depends on the relative stress gradient $\chi^* = {}^1\!/\!_{\sigma_{max}} \frac{d\sigma}{dx}$ (see Figure 14) and on the material and expresses the increase of the fatigue stress limit due to the presence of a stress gradient.

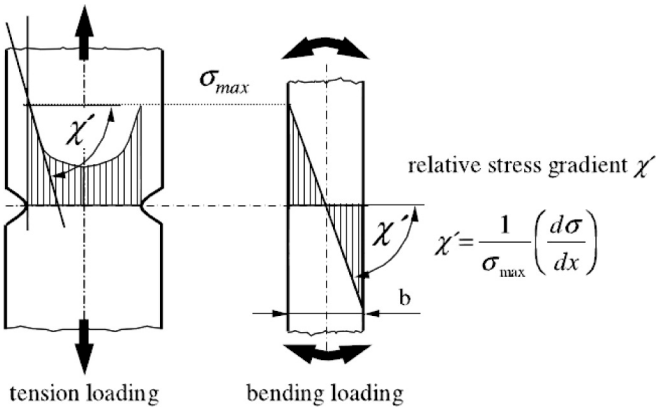

Figure 14. Relative stress gradient for tension loading of a notched specimen and bending of an unnotched specimen - adapted from [18].

As shown in Figure 14, the stress gradient can be related either to the geometry of the notch or the type of loading.

The notch support factor is related to the relative stress gradient through the following relation [18]:

$$\eta_\chi = 1 + \left(\frac{\sigma_{bf}}{\sigma_{af}} - 1\right)\left(\frac{\chi^*}{{}^2\!/\!_b}\right)^{K_D} \tag{4}$$

Where $\frac{\sigma_{bf}}{\sigma_{af}}$ is the ratio of the bending and axial fatigue limits, b is the dimension of the specimen while KD is an exponent that depends on the material [19]. Relation 4 expresses that as the local stress gradient increases, the material is able to withstand a higher stress before a damage occurs. The denominator ${}^2\!/\!_b$ expresses the relative stress gradient of a bending specimen with dimension b (Figure 14). The exponent K_D is taken from experimental data available in the literature [19], which state that the increase in the fatigue strength is less than linear with the relative stress gradient.

The stress gradient field can be computed from FE results by writing the second derivatives of the element shape functions [20]. By considering isoparametric elements the relation between the second parametric derivatives and the physical derivatives reads

$$\begin{bmatrix} {}^{\partial^2 N_i}\!/\!_{\partial\xi^2} \\ {}^{\partial^2 N_i}\!/\!_{\partial\eta^2} \\ {}^{\partial^2 N_i}\!/\!_{\partial\zeta^2} \\ {}^{\partial^2 N_i}\!/\!_{\partial\xi\partial\eta} \\ {}^{\partial^2 N_i}\!/\!_{\partial\xi\partial\zeta} \\ {}^{\partial^2 N_i}\!/\!_{\partial\eta\partial\zeta} \end{bmatrix} = [H]_{6x3} \begin{bmatrix} {}^{\partial N_i}\!/\!_{\partial x} \\ {}^{\partial N_i}\!/\!_{\partial y} \\ {}^{\partial N_i}\!/\!_{\partial z} \end{bmatrix} + [J^2]_{6x6} \begin{bmatrix} {}^{\partial^2 N_i}\!/\!_{\partial x^2} \\ {}^{\partial^2 N_i}\!/\!_{\partial y^2} \\ {}^{\partial^2 N_i}\!/\!_{\partial z^2} \\ {}^{\partial^2 N_i}\!/\!_{\partial x\partial y} \\ {}^{\partial^2 N_i}\!/\!_{\partial x\partial z} \\ {}^{\partial^2 N_i}\!/\!_{\partial y\partial z} \end{bmatrix} \tag{5}$$

matrices $[H]$ and $[J^2]$ contains respectively the second and the first derivatives of shape functions in the parametric space (see [20] for details).

Taking for example the gradient of the strain component e_{11} we have

$$\nabla e_{11} = \begin{bmatrix} \partial e_{11}/\partial x \\ \partial e_{11}/\partial y \\ \partial e_{11}/\partial z \end{bmatrix}^T = \begin{bmatrix} \sum_i u_i \frac{\partial^2 N_i}{\partial x^2} \\ \sum_i u_i \frac{\partial^2 N_i}{\partial x \partial y} \\ \sum_i u_i \frac{\partial^2 N_i}{\partial x \partial z} \end{bmatrix}^T \quad (6)$$

and the gradient of the stress component σ_{11} can be then computed through the material constitutive law.

After computing the stress gradient field on the entire wheel the local notch support factor can be calculated and the stress-life curve can be corrected according to the obtained value (Figure 15).

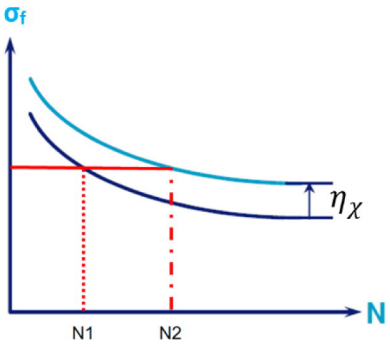

Figure 15. Stress-life correction according to the notch support factor.

The computed fatigue life of the wheel after the gradient correction shows a better agreement with experimental results as shown in Figure 16. If a small area around the critical location is considered, the estimated number of cycles before a damage nucleation is about 10^6 cycles. The fatigue life is still underestimated with respect to experimental data, however this was quite expected since the crack propagation contribution is not considered in the model.

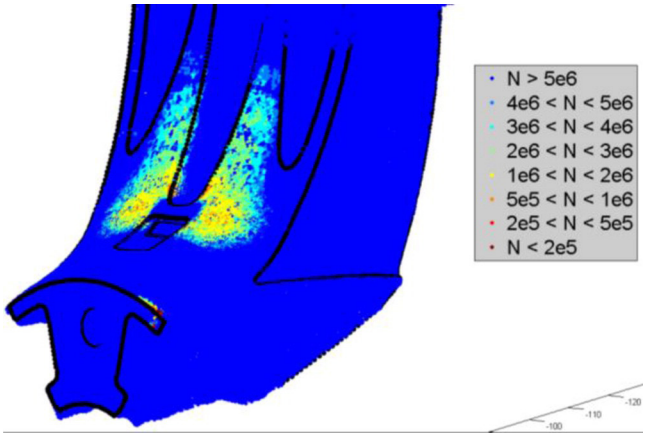

Figure 16. Contour plot of fatigue life of the wheel with the Sines criterion corrected with stress gradient.

Conclusions

In the paper the fatigue properties of aluminum wheels have been discussed. Fatigue data of the A356 T6 aluminum alloy have been derived from experimental tests. Cylindrical specimens have been extracted from different zones of the wheel. Strain-controlled and load-controlled tension-compression cyclic tests have been carried on and the strain-life and stress-life curves of the material have been computed. Results show very little variability of the fatigue performances in the medium-high cycle ranges among the different areas of the wheel. The rotary bending fatigue test of the wheel has been simulated by means of Finite Elements. The FE model has been experimentally validated by measuring the deformations acting at the most stressed areas of the wheel during the test. Strain gauges have been employed for measuring the strain during the fatigue test of the wheel. Results from simulations showed a good agreement with measured values, with a maximum error below 10% of the maximum measured value. The validated numerical model has been employed for estimating the fatigue life of the wheel. Multiaxial fatigue criteria have been adopted, namely the Sines criterion and Matake criterion. Both of the methods identify the same region as the most critical for the damage nucleation. The location of cracks was confirmed by experimental tests on actual wheels, however both of the methods are too conservative regarding the fatigue life prediction. A correction of the material fatigue strength based on the local stress gradient at the notches has been proposed. The stress gradient field has been computed by writing the second derivatives of the element shape functions and the notch support factor has been calculated. The local fatigue strength of the material has been corrected according to the computed notch support factor. The correction in the critical area of the wheel was about 20% on the stress limit. Results exhibit a better agreement with experimental data.

The proposed method has proved to be effective for the design of a component of primal importance for the safety of the vehicle.

References

1. Mastinu G., Ploechl M., “Road and off-road Vehicle System Dynamic Handbook, CRC Press, (2014).
2. Scheibe F., Smith M.C., “Analytical solutions for optimal ride comfort and tyre grip for passive vehicle suspensions, International Journal of Vehicle Mechanics and Mobility, 47, 1229-1252 (2009).
3. Li P., Maijer D.M., Lindley T.C., Lee P.D., “A through process model of the impact of in-service loading, residual stresses, and microstructure on the final fatigue life of an A356 automotive wheel”, Materials Science and Engineering, A 460-461, 20-30 (2007).
4. Fischer, G. and Grubisic, V., "Design Criteria and Durability Approval of Wheel Hubs," SAE Technical Paper 982840, 1998, doi:10.4271/982840.
5. Raju P.R., Satyanarayana B., Ramji K., Babu K.S., “Evaluation of fatigue life of aluminium alloy wheels under bending loads”, Fatigue and Fracture of Engineering Materials and Structures, DOI: 10.1111/j.1460-2695.2008.01316.x (2008).

6. Wang L., Chen Y., Wang C., Wang Q., “Fatigue life analysis of aluminum wheels by simulation of rotary fatigue test”, Journal of Mechanical Engineering, 57, 31-39 (2011).
7. Kocabicak U., Firat M., “Numerical analysis of wheel cornering fatigue tests”, Engineering Failure Analysis, 8, 339-354 (2001).
8. Kocabicak U., Firat M., “A simple approach for multiaxial fatigue damage prediction based on FEM post-processing”, Materials and Design, 25, 73-82 (2004).
9. Zheng Z., Sun T., Xu X., Pan S., Yuan S., “Numerical simulation of steel wheel dynamic cornering fatigue test”, Engineering Failure Analysis, 39, 124-134 (2014).
10. ASTM E606/E606M - 12, “Standard test method for strain-controlled fatigue testing”, ASTM International (2012).
11. ISO 12106:2003, “Metallic materials - fatigue testing - axial strain-controlled method” (2003).
12. SAE International Surface Vehicle Standard, "Wheels - Passenger Car and Truck Performance Requirements and Test Procedures," SAE Standard J328, Rev. Feb 2005.
13. Satyanarayana N., Sambaiah Ch., “Fatigue analysis of aluminium alloy wheel under radial load”, International Journal of Mechanical and Industrial Engineering, ISSN No. 2231 -6477, Vol-2, Issue-1 (2012).
14. Papadopoulos I.V., Davoli P., Gorla C., Filippini M., Bernasconi A., “A comparative study of multiaxial high-cycle fatigue criteria for metals”, International Journal of Fatigue, Vol. 19, No.3, 219-235 (1997).
15. Suresh S., “Fatigue of Materials - second edition”, Cambridge University Press (1998).
16. Gobbi, M., Mastinu, G., Ballo, F., and Previati, G., "Race Motorcycle Smart Wheel," *SAE Int. J. Passeng. Cars - Mech. Syst.* 8(1):119-127, 2015, doi:10.4271/2015-01-1520.
17. Karolczuk A., Macha E., “A review of critical plane orientations in multiaxial fatigue failure criteria of metallic materials”, International Journal of Fracture, 134, 267-304 (2005).
18. Eichlseder W., “Fatigue analysis by local stress concept based on finite element results”, Computers and Structures, 80, 2109-2113 (2002).
19. Eichlseder W., “Lebensdauervorhersage auf Basis von Finite Elemente Ergebnissen”, Mat.-wiss. U. Wrkstofftech., 34, 843-849 (2003).
20. Xing J., Zheng G., “Stress Field Gradient Analysis Technique Using Lower-Order C^0 Elements”, Mathematical Problems in Engineering, Volume 2015, http://dx.doi.org/10.1155/2015/457046 (2015).
21. Patel H., Satankar R.K., “A review on fatigue life prediction of a heavy vehicle steel wheel by using finite element analysis”, International Journal of Engineering Sciences & Research Technology, 3(6), 435-438 (2014).
22. Meng J., Zhu P., Liu Z., Ji Q., “Integration of multi-step stamping effects in the bending fatigue analysis of a steel wheel”, Fatigue & Fracture of Engineering Materials & Structures, 36, 795-808 (2013).
23. Wang X., Zhang X., “Simulation of dynamic cornering fatigue test of a steel passenger car wheel”, International Journal of Fatigue, 32, 434-442 (2010).
24. Carboni M., Beretta S., Finzi A., “Defects and in-service fatigue life of truck wheels”, Engineering Failure Analysis, 10, 45-57 (2003).
25. Lin G., Pang H., Zhang W., Wang D., Feng L., “A self-decoupled three-axis force sensor for measuring the wheel force”, Proc IMechE Part D: J Automobile Engineering, Vol 228(3), 319-334 (2014).
26. http://www.kistler.com/ Kistler (RoaDyn Wheel Force Sensor), 5/2005.
27. http://ww.mts.com/ MTS System Corporation (SWIFT Wheel Force Transducer), 5/2005.
28. Gobbi M., Mastinu G., Rocca G., “A smart wheel for improving the active safety of road vehicles”, Proceedings of the 2010 International Design Engineering Technical Conference, Montreal, Canada (2010).
29. Ballo F., Gobbi M., Mastinu G., Previati G., “Advances in Force and Moments Measurements by an Innovative Six-axis Load Cell”, Experimental Mechanics, 54, 571-592, DOI 10.1007/s11340-013-9824-4, (2014).
30. Gobbi M., Mastinu G., “Analytical description and optimization of the dynamic behaviour of passively suspended road vehicles”, Journal of Sounds and Vibrations, 245, 457-481 (2001).
31. Wiedemann J., “Leichtbau, Elemente und Konstruktion”, Springer, (2007).
32. Campbell F.C., “Lightweight Materials: Understanding the Basics”, ASM International, (2012).
33. Nurkala, L. and Wallace, R., "Development of the SAE Biaxial Wheel Test Load File," SAE Technical Paper 2004-01-1578, 2004, doi:10.4271/2004-01-1578.
34. Archibald, K., Schnaidt, W., Wallace, R., and Archibald, K., "Minimum Cycle Requirement for SAE J2562," SAE Technical Paper 2014-01-0073, 2014, doi:10.4271/2014-01-0073.
35. Zhang B., Cockcroft S.L., Maijer D.M., Zhu J.D., Phillion A.B., “Casting defects in low-pressure die-cast aluminum alloy wheels”, JOM, Vol. 57, Issue 11, 36-43 (2005).
36. Murakami Y., Metal Fatigue: Effects of small defects and nonmetallic inclusions”, Elsevier (2002).

37. Wang Q.G., Apelian D., Lados D.A., “Fatigue behavior of A356-T6 aluminum cast alloys. Part I. Effect of casting defects”, Journal of Light Metals, 1, 73-84 (2001).
38. www.cromodorawheels.it, Cromodora Wheels, aluminum alloy wheels manufacturer.

Contact information

Federico Ballo, Politecnico di Milano
federicomaria.ballo@polimi.it
phone: +39 02 2399 8606